Assembling Nonspherical 2D Binary Nanoparticle Superlattices by Opposite Electrical Charges: The Role of Coulomb Forces

Zhaoyong Sun,[†] Zhiping Luo,[‡,*] and Jiye Fang[†,*]

[†]Department of Chemistry, State University of New York at Binghamton, Binghamton, New York 13902 and [‡]Microscopy and Imaging Center, Texas A&M University, College Station, Texas 77843

ABSTRACT High-quality ~16 nm c-In_2O_3 nanoctahedra and ~6 nm Pd spherical nanoparticles were synthesized *via* a high-temperature wet-chemical approach, and their electrophoretic mobilities in toluene were investigated, respectively. Opposite electrical charge-induced 2D binary nanoparticle superlattice patterns containing two such nanocomponents were prepared, for the first time. Three types of c-In_2O_3-skeleton-structure-contained assembly patterns were identified as well. It was further observed that the vertices of c-In_2O_3 nanoctahedra could have higher electrical charge density than that on edge or plane and the small Pd nanoparticles were "suspended" on the middle plane of the c-In_2O_3 nanoctahedra, apparently well above the substrate surface (support film) rather than sitting on it. The assembly structure study indicates that Coulomb forces resulted from the opposite electrical charges are the dominative driving forces to induce the formation of such nanoctahedra-nanospheres 2D binary nanoparticle superlattices.

KEYWORDS: nanoctahedron · binary nanoparticle superlattice · opposite electrical charge · self-assembly · electrophoretic mobility · indium oxide · electron microscopy

It is now possible to fabricate nanoparticles (NPs) with precisely controllable size and shape using a wet-chemical synthesis approach.[1−7] Using these high-quality NPs as a set of "building blocks", success has also been demonstrated with the packing 2- and 3D NP arrays with properties of both fundamental and practical interest.[8−14] Recently, it was reported that various low-density spherical binary nanoparticle superlattices (BNSLs) patterns could be achieved through opposite electrical charges on the NPs from different capping ligands.[15,16] Although the packing symmetry as a function of the size ratio between the small and large NPs was extensively studied[9,10,15,17−19] and the investigation has even been extended to a ternary system,[20] observation of BNSLs containing nonspherical NPs still remains a challenge.

It is known that the shape, size, surface facet, and structural assemblies of NPs play significant roles in their potential performance, such as electrocatalytic activity,[1,3] crystal durability,[21] reaction selectivity,[22−24] magnetic behavior,[25] and photovoltaic conversion efficiency.[26−29] Unlike spherical NPs which are randomly oriented when being assembled into a supercrystal, the superlattices assembled by nonspherical NPs may offer certain enhanced characteristics with their anisotropic nanostructure, such as unusual magnetization and enhanced catalytic performance due to their aligned geometric axes of each unit. We previously reported a success in preparation of self-assembled superlattices containing octahedral cubic-phase In_2O_3 (c-In_2O_3) nanocrystals, and our observation of three packing structures.[30] As an extension, in this article we report, for the first time, on an observation of 2D BNSLs consisting of c-In_2O_3 nanoctahedra and Pd nanospheres through opposite electrical charges. Structural analyses of these 2D BNSLs amazingly reveal that most of the Pd NPs "suspend" on the middle plane of the c-In_2O_3 nanoctahedra rather than sitting on the substrate surface, and the locations of Pd NPs are dependent on the c-In_2O_3 orientation structures. On the basis of these observations, we propose that Coulomb forces from opposite electrical charges on c-In_2O_3 nanoctahedra and Pd NPs rather than other interactions such as van der Walls, steric, or dipolar interparticle forces are the major driving forces to induce the assembly of packing a specific 2D BNSL pattern. Investigation of such 2D patterns formed from nonspherical building blocks is noteworthy in aspects of NP interaction study as well as potential development of novel meta-materials.

*Address correspondence to jfang@binghamton.edu (synthesis/assembly/charge characterization), luo@mic.tamu.edu (TEM/STEM/EDS/tomography evaluation).

Received for review August 20, 2009 and accepted March 18, 2010.

Published online March 29, 2010.
10.1021/nn100302v

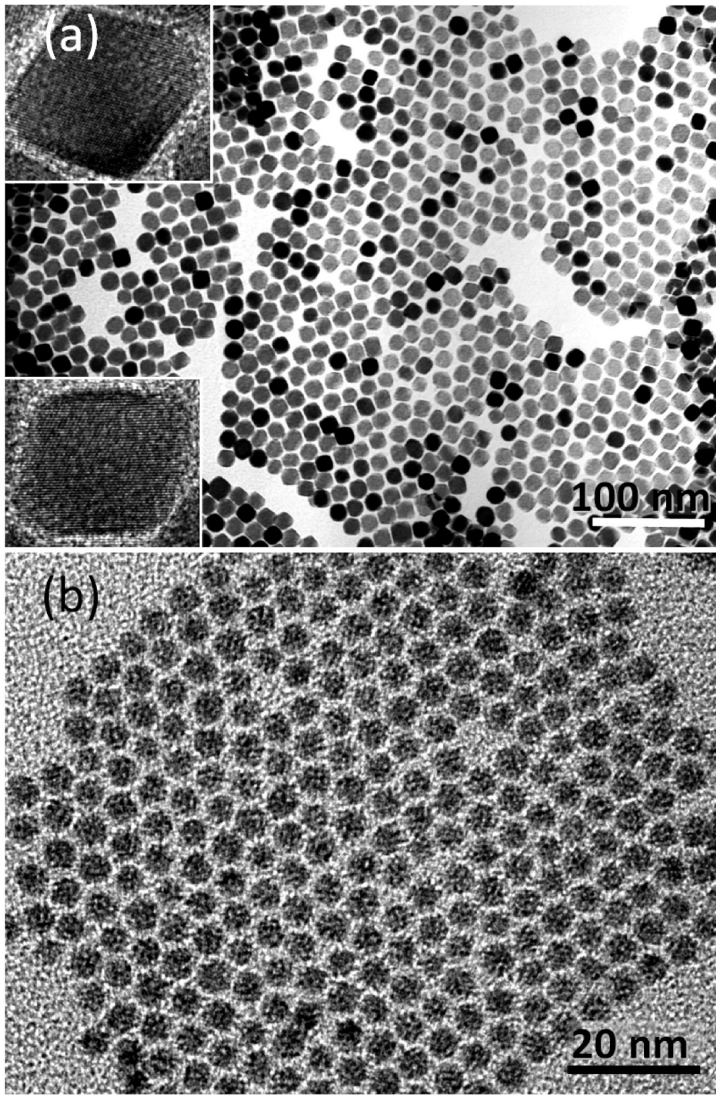

Figure 1. TEM images of the starting materials: (a) c-In_2O_3 nanoctahedra with two enlargements inserted; (b) spherical Pd nanoparticles.

RESULTS AND DISCUSSION

Cubic-phase In_2O_3 (c-In_2O_3) nanoctahedra[30] and spherical Pd NPs[31] were rationally synthesized by adopting methods reported previously. As shown in Figure 1, the size of c-In_2O_3 and Pd NPs from the typical syntheses were determined as 15.9 $\pm$ 1.2 nm (diagonal length) and 5.8 $\pm$ 0.4 nm (spherical diameter), respectively, on the basis of transmission electron microscopic (TEM) images.

The as-synthesized c-In_2O_3 nanoctahedra capped with oleic acid (OA) and oleylamine (OAm) were washed using anhydrous ethanol and then redispersed in toluene, whereas a ligand-exchange process was applied to Pd NP suspension as the following description. The as-synthesized spherical Pd NPs originally capped with trioctylphosphine (TOP) and OAm underwent a capping-agent-exchange post-treatment with 1-dodecanethiol in toluene.[31] During this process (the details of preparation and post-treatment procedure can be referred to the section of "experimental details"), TOP and OAm on the surface of the Pd NPs are assumed to be replaced by 1-dodecanethiol. As reported earlier, it is believed that electrical charges might exist on sterically stabilized NPs even in a nonpolar solvent.[32−34] According to the literature,[15] it is anticipated that the OA-capped c-In_2O_3 nanoctahedral and thiol-capped Pd NP colloids in toluene carry positive and negative charges, respectively. Usually, the electrical charge (*Z*, in unit of *e*) on a NP in a low dielectric solvent without electrolyte is proportional to the electrophoretic mobility (μ_e) through a relationship

$$Ze = 3\pi\eta a\mu_e$$

where η is the viscosity of the solvent and *a* is the hydrodynamic diameter of a spherical or sphere-like NP.[35] To verify this conjecture of opposite electrical charges presented in both types of suspensions, distributions of electrophoretic mobility of both colloidal suspensions were measured using a Malvern Zetasizer Nano ZS instrument (Malvern Instruments) in which a laser doppler working mechanism was adopted. Figure 2a,b presents the peaks of electrophoretic mobility distribution of c-In_2O_3 nanoctahedral colloids and Pd NP colloids in toluene, respectively. Figure 2a shows a peak with a positive mobility value ($\sim$0.035 μm cm V^{-1} s^{-1}) for 16 nm c-In_2O_3 nanoctahedra in toluene, indicating the presence of positive charges on these nanoctahedra in such a colloidal suspension. In contrast, an observation of a peak with a negative mobility value (*ca.* $-$0.075 μm cm V^{-1} s^{-1}) for 6 nm spherical Pd NPs in toluene implies that these NPs possess negative charges (see Figure 2b).[15] This experimental survey confirms the existence of different electrical charges on both "precursor" suspensions used for the preparation of 2D BNSLs in this work.

The c-In_2O_3−Pd colloidal suspensions were prepared by mixing the preprepared c-In_2O_3 stock toluene-suspension and Pd stock toluene-suspension, while the molar ratio between c-In_2O_3 and Pd in toluene was maintained around 4.8:1. Prior to an assembly of this mixture on a TEM grid, one drop of oleic acid was introduced in order to increase the population of positively charged oxide NPs and to oppositely affect the electrical charge on metallic NPs, as pointed out previously.[15] It is believed that interactions from opposite electrical charges on NPs, rather than other relatively weaker interactions such as van der Waals forces, steric or dipolar interparticle interactions, are the major driving forces to form 2D BNSLs.[15] BNSLs of c-In_2O_3 and Pd were then achieved by simply dropping the suspensions on copper TEM grids coated with Formvar/carbon and analyzed using a Hitachi H-7000 TEM and FEI Tecnai G^2 F20 FE-TEM with scanning TEM (STEM), energy dispersive X-ray spectroscopy (EDS), and electron tomography capabilities.

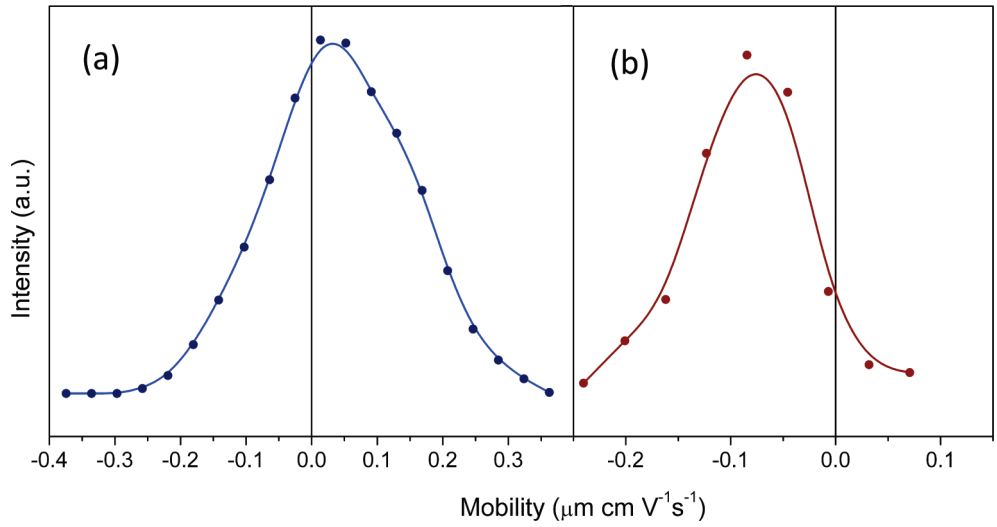

Figure 2. Electrophoretic mobilities of (a) c-In_2O_3 nanoctahedra and (b) Pd nanoparticles in toluene.

The structure of c-In_2O_3−Pd 2D BNSLs strongly depends on the assembly configuration of the c-In_2O_3 nanoctahedron component as a "skeleton pattern". As shown in TEM projection images (Figure 3a,b, also refer to Figure S1 in Supporting Information), two types of individual c-In_2O_3−Pd structures were observed. In Figure 3a, the c-In_2O_3 nanoctahedra are ⟨001⟩-projected and orientated by sitting on their vertices. The Pd NPs are "inserted" at positions that close to four vertices from the four nearest-neighbor c-In_2O_3 nanoctahedra. In this pattern, the c-In_2O_3 nanoctahedra are oriented along ⟨001⟩, which is similar to the Type-I packing structure in assembly of pure c-In_2O_3 nanoctahedra.[30] Figure 3c is a large-area TEM projection image, demonstrating a Type-I-dominated 2D BNSL structure. We observed that different 2D BNSL structures could exist simultaneously on the same substrate. Interestingly, Figure 3b reveals the second type of packing arrays. The c-In_2O_3 nanoctahedra, projected in ⟨110⟩ orientation, sit on their edges, that is, slightly truncated (110) facets. This kind of assembly structure was previously observed in the case of pure c-In_2O_3 nanoctahedron patterns[30] and was attributed to a Type-II pattern.[30] The rows of c-In_2O_3 nanoctahedra in this Type-II structure are half-side-length shifted from each other (*i.e.*, the next row is placed by shifting a half-NP distance along the direction of the row axis) in order to maximize the surface contact. Since the amount of electrical charges in each unit of c-In_2O_3 in such a pattern is relatively weak (*vide infra*), in most cases the Pd NPs are only introduced in the positions between the vertices of any two neighboring c-In_2O_3 nanoctahedra in a row rather than vacancies between the rows. In both Type-I and Type-II structures, the distances of c-In_2O_3 interparticles increase in comparison with the case of the single c-In_2O_3 nanoctahedron pattern[30] possibly due to the inclusion of Pd NPs into the c-In_2O_3 lattice. It is also worth

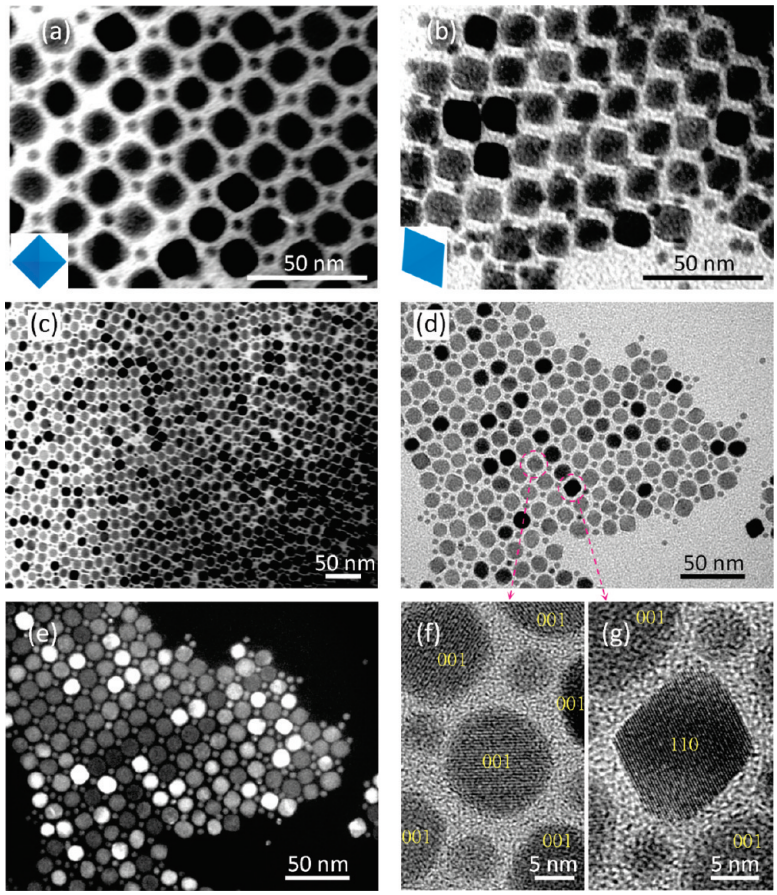

Figure 3. TEM images of binary assembly structures formed between c-In_2O_3 nanoctahedra and Pd nanoparticles: (a) Type-I assembly, the nanoctahedra oriented along ⟨001⟩, as indicated by the inserted model; (b) Type-II assembly, the nanoctahedra oriented along ⟨110⟩, as indicated by the model; (c) large-area Type-I assembly; (d) bright-field image of an example of mixed Type-I and Type-II assemblies; (e) dark-field image of the area in panel d; (f) enlarged one (high-resolution TEM) from circled area in panel d, Type-I; (g) enlarged one from circled area in panel d, Type-II.

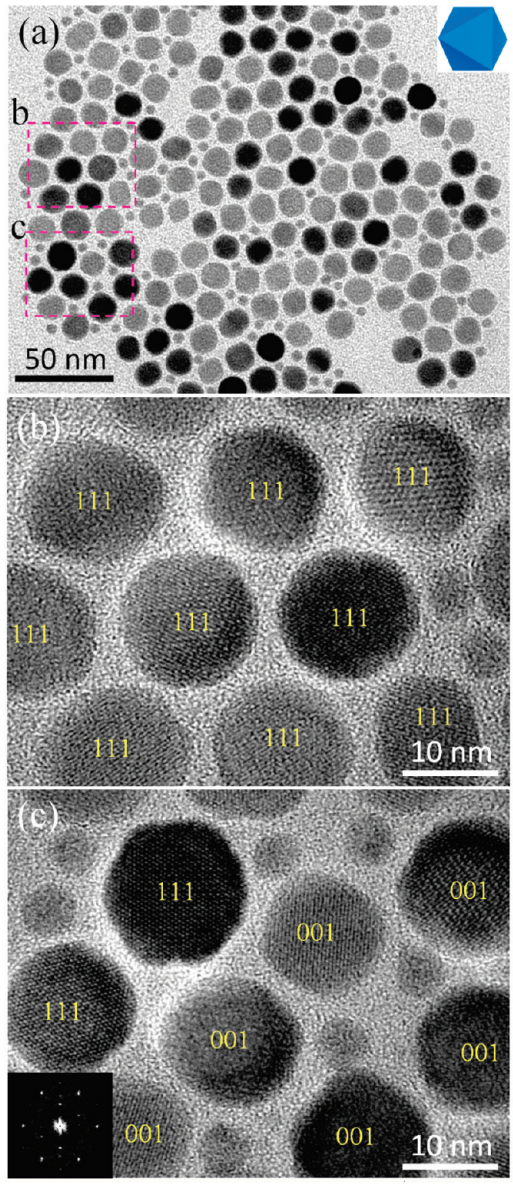

Figure 4. TEM images of (a) Type-III assembly, the c-In_2O_3 nanoctahedra oriented along ⟨111⟩, as indicated by the inserted model; (b) high-resolution image from panel a showing ⟨111⟩ oriented c-In_2O_3 nanoctahedra; (c) high-resolution image from panel a showing ⟨111⟩ and ⟨001⟩ oriented c-In_2O_3 nanoctahedra. An FFT pattern of a ⟨111⟩ nanoctahedron is inserted. Note the absence of Pd particles around the ⟨111⟩ oriented c-In_2O_3 nanoctahedra.

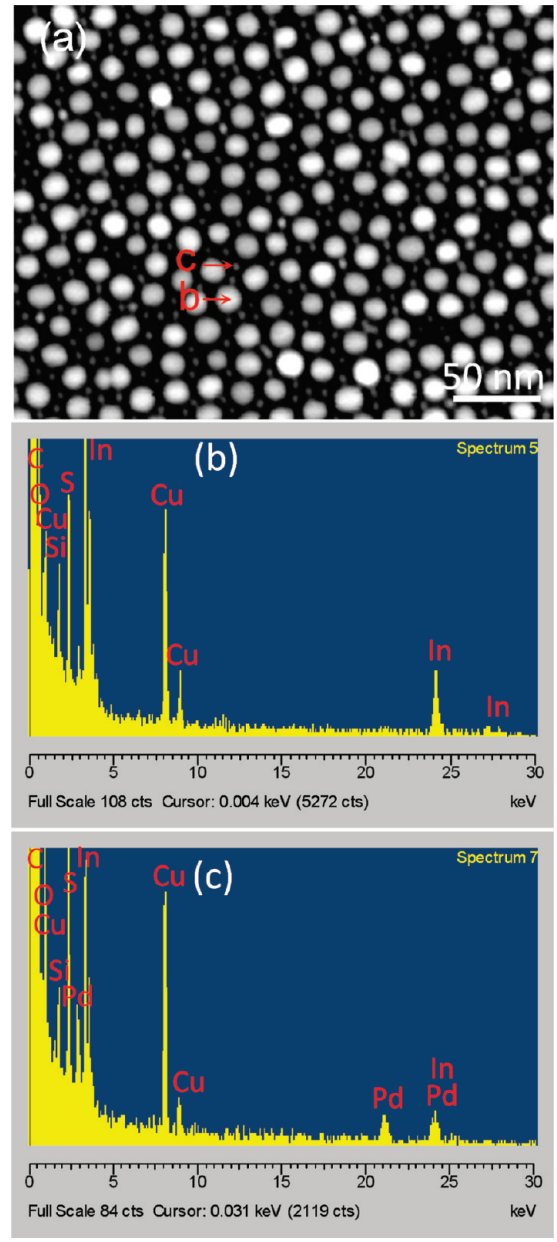

Figure 5. STEM image (a), where two single Pd and In_2O_3 particles, labeled as "b" and "c", are selected for EDS analysis in panels b and c, respectively. The horizontal axis of the EDS spectra is energy in keV, and the vertical axis, counts.

mentioning that, in many cases as shown in Figure 3d−g, a mixed structure containing both Type-I and Type-II could be determined.

In our previous study in a single c-In_2O_3 nanoctahedron assembly system,[30] we have determined a third type of assembly structure, oriented along ⟨111⟩ and designated as "Type III". That is, all of the c-In_2O_3 nanoctahedra sit on the substrate by their (111) facets and the projection direction is [111]. In this c-In_2O_3 nanoctahedron-Pd NP binary 2D assembly system, we attempted to identify the similar c-In_2O_3 pattern as a skeleton structure in the binary system. As illustrated in Figure 4a, instead of a single Type-III skeleton c-In_2O_3 nanoctahedron pattern, a structure-mixed pattern containing Type-III and Type I c-In_2O_3 was observed. From high-resolution TEM images in Figure 4b,c, it was confirmed that Pd NPs only exist around Type I-oriented c-In_2O_3 nanoctahedra, and no Pd NP was detected around the Type III-oriented c-In_2O_3 nanoctahedra. This observation further supports the inference that the opposite electrical charges are the major driving forces for the 2D BNSL formation. In Type I-oriented c-In_2O_3 pattern, each c-In_2O_3 nanoctahedron contacts the substrate surface (the TEM support film) through only one vertex. The minimum contacting area ensures that most of the positive electrical charge is "isolated" on the surface of the c-In_2O_3 nanoctahedron, attracting

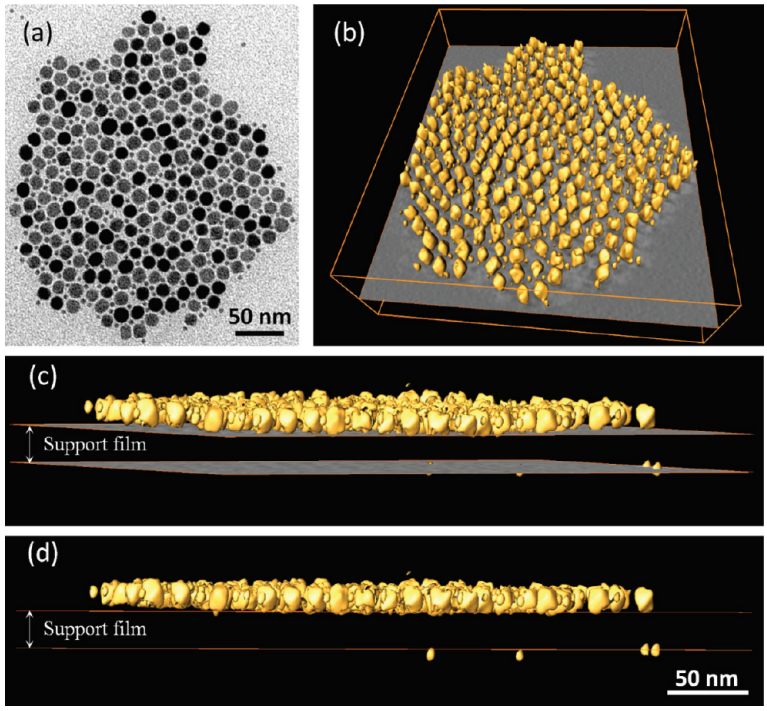

Figure 6. 3D reconstruction: (a) TEM image; (b) reconstructed volume rendering; (c) close to edge-on side view of the volume; (d) edge-on side view of the volume. Data bars represent a scale of 50 nm.

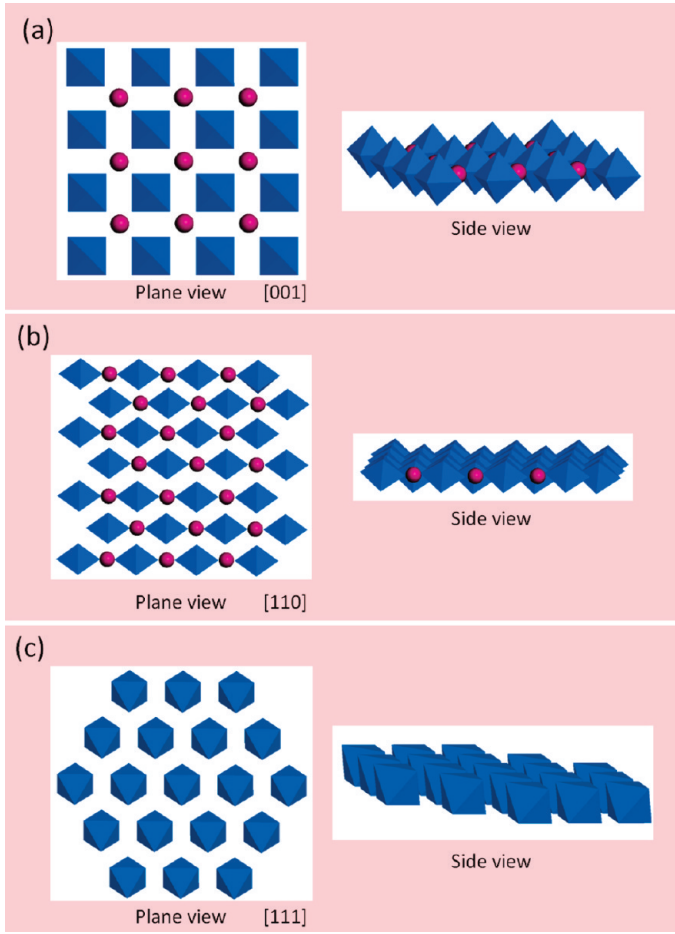

Figure 7. Structure models of (a) Type I ([100] oriented), (b) Type II ([110] oriented), and (c) Type III ([111] oriented) 2D BNSL assemblies along plane and side views, respectively.

a maximum number of opposite charge carriers, that is, four Pd NPs, around it (Figure 3a). In Type II-oriented c-In_2O_3 pattern, each c-In_2O_3 nanoctahedron contacts the substrate surface through a nanoctahedral edge. In comparison with the vertex, the increased contacting area on edge allows a partial loss of the positive electrical charge from the c-In_2O_3 nanoctahedron, resulting in a less number of opposite charge carriers, that is, two Pd NPs, around it (Figure 3b). In Type III-oriented c-In_2O_3 pattern, the contact through a triangular face for each c-In_2O_3 nanoctahedron maximizes the transfer of the positive electrical charge from c-In_2O_3 to the substrate surface with minimum positive charge remaining. This explains why no Pd NP could be "attracted" around the Type III-oriented c-In_2O_3 nanoctahedra (Figure 4b,c).

To identify the compositions of the 2D BNSL pattern, a STEM image, taken using a spot size of 1 nm, is shown in Figure 5a. Two types of NPs, labeled as "b" and "c" respectively, are selected for the EDS analysis in the STEM mode. Despite of the elements induced by the chemicals during the sample preparation as well as Cu signals from the grid, the EDS spectrum from the large particle presents In and O signals without Pd (Figure 5b), whereas that from the small particle shows the evidence of Pd (Figure 5c), although spurious In signals from the surrounding large particles that are hard to avoid are also present.[36] The EDS analysis is consistent with the assumption that the large NPs are In_2O_3 and small NPs are Pd. However, it is still ambiguous about the position of Pd NPs in the projection direction (the direction perpendicular to plane of the substrate) based on these 2D images. The Pd NPs may be just "inserted" among the c-In_2O_3 nanoctahedra and sterically assembled on the substrate plane, or separated from the substrate surface and "suspended" in the projection direction among the c-In_2O_3 nanoc-

tahedra due to the interaction of opposite electrical charges. To explore this, 3D reconstruction using tomography was carried out.

Figure 6a presents a Type-I/Type-II-mixed 2D BNSL area selected for the tomography. A series of images at different angles were taken (refer to Figure S2 in Supporting Information), and they were then reconstructed by the backprojection method using the FEI Xplore3D program. Figure 6b shows a reconstructed volume that was rendered using Isosurface, indicating NPs that are consistent with those observed in the real TEM image in Figure 6a. Using this reconstructed volume, it is possible to visualize the pattern at any angles. To determine the relative positions of Pd NPs to c-In_2O_3 nanoctahedra, it is necessary to tilt this volume to the edge-on angle (perpendicular to the electron beam). Figure 6c and 6d are two representative side views, near and at the edge-on positions, respectively. It is clear that most of the Pd NPs locate on the middle plane of the c-In_2O_3 nanoctahedra, apparently well above the substrate surface (support film) rather than sitting on it. A movie demonstrating the continuous turning near this edge-on side view angle is provided in the Supporting Information. Note that in this area, a few Pd NPs are found on another side of the support film, and thus two planes are shown in Figure 6c and 6d, depicting the top and bottom surfaces of the support film. Supposing the bottom few Pd NPs attach the support film due to the absence of charge on this side, the support film thickness is estimated as 17 nm, consistent with the support film thickness given by the vendor Ted Pella.

In the cases of BNSLs containing all-spherical NPs studied previously,[15,16] electrical charges should distribute on the surfaces of spherical NPs homogeneously. However, the electrical charge density on surface of a nanoctahedron would not be even. In physics, it is well-known that a charged asymmetric object has the strongest electric field near its part that has the smallest radius of curvature.[37] According to this principle, the vertices are expected to have higher charge density than that on edge or plane of a nanoctahedron. Exploration of Pd positions in our experiments apparently verifies this assumption. On the other hand, the success of 2D BNSL assembly is dependent on the amount of electrical charges remaining on the c-In_2O_3 nanoctahedra, which is up to the contact area between a nanoctahedron and the substrate surface. As summarized in the three structural models based on the experimental observations in Figure 7, the coordination number of Pd NPs around a c-In_2O_3 nanoctahedron is ultimately dependent on the packing orientation of the c-In_2O_3 nanoctahedron.

CONCLUSIONS

We have identified opposite electrophoretic mobilities of ~16 nm c-In_2O_3 nanoctahedra and ~6 nm Pd NPs in toluene, and for the first time, demonstrated nonspherical 2D BNSL assembly patterns containing the mentioned building blocks. Three types of c-In_2O_3 skeleton structures were observed in the 2D octahedral c-In_2O_3-spherical Pd NP BNSL assembly patterns. It was further determined that (1) the vertices of c-In_2O_3 nanoctahedra could have higher electrical charge density than that on edge or plane; (2) most of the Pd NPs locate on the middle plane of the c-In_2O_3 nanoctahedra well above the substrate surface (support film) rather than sitting on it in the 2D BNSL assembly patterns; (3) the orientation of c-In_2O_3 nanoctahedra dominates the structure of a nonspherical 2D BNSL pattern. On the basis of these investigations, we propose that Coulomb forces resulted from the opposite electrical charges on c-In_2O_3 and Pd NPs are the major driving forces to induce the assembly, and the c-In_2O_3 skeleton orientation structures are crucial to the formation of a 2D BNSL pattern. The preparation and study of such nonspherical BNSL systems can provide a general and inexpensive path to meta-materials with precisely tuned chemical composition, controlled structure of building block assembly, and combined properties. It is noteworthy in aspects of NP interaction investigation as well as potential novel meta-materials engineering.

EXPERIMENTAL DETAILS

Preparation of Cubic Phase c-In_2O_3 Nanoctahedra. A 0.42 mmol portion of indium acetate (99.99%, Alfa Aesar), 0.60 mL of oleic acid (90%, Sigma-Aldrich), and 0.55 mL of oleylamine (70%, Sigma-Aldrich) were mixed with 7.0 mL of hexadecane (99+%, Sigma-Aldrich) in a three-neck round-bottom flask equipped with a condenser. Standard air-free techniques were used, and the mildly stirred mixture was vacuumed at room temperature for 15 min. After being purged twice with argon gas, the mixture was heated to 110 °C and kept at that temperature for 70 min within the vacuum. Then 1.5 mmol of trimethylamine N-oxide (TMNO, 98%, Sigma-Aldrich) was added into the vigorously stirred mixture under an argon stream after the mixture temperature was reduced to 100 °C. The system was then heated to 290 °C and refluxed for 2 h while a dynamic multiple-injection operation was also applied. The resulting turbid mixture was cooled down to room temperature. The c-In_2O_3 nanocrystals, which are a gray precipitate and can be completely dispersed in hexane, were separated from the reaction mixture by adding sufficient amounts of anhydrous ethanol and collected by a subsequent centrifugation. Highly monodisperse c-In_2O_3 nanoctahedron suspensions could be obtained after a standard size-selection post-treatment using a pair-solvent of anhydrous hexane (98.5%, BDH) and anhydrous ethanol (200 proof, AAPER).

Preparation of Spherical Pd Nanoparticles. A 0.1 g portion of palladium(II) acetylacetonate [Pd(acac)$_2$] (34.8−35.0% Pd, Gelest) was added into 1.0 mL of trioctylphosphine (TOP, 90%, Aldrich) to form orange Pd−metal complexes. The metal complex solution was then added to 10 mL of oleylamine (70%, Sigma-Aldrich). Subsequently, the resultant solution was slowly heated to 250 °C and kept at this temperature for 30 min under vigorous agitation and argon protection. During this process, the initial orange color of the solution gradually turned dark brown. These colloids were cooled to room temperature and anhydrous etha-

nol (200 proof, AAPER) was added to yield a black precipitate, which was subsequently isolated by centrifugation. Homogeneous spherical Pd nanoparticles suspended in hexane can be further obtained after a size-selection post-treatment mentioned above.

Molar Concentration Estimate in Toluene Stock Suspensions. (1) The monodisperse c-In_2O_3 nanoctahedra in hexane capped with oleic acid and oleylamine were isolated by precipitating the suspensions using a sufficient amount of anhydrous ethanol followed by centrifugation. The precipitates were then transferred in toluene. A 1.0 mL portion of c-In_2O_3 toluene suspension was added into a small clean vial which was preweighed exactly before drying. After the solvent of the sample was gradually evaporated in a vacuum oven, the vial was transferred into a tube-furnace and heated to 600 °C under an air stream to completely remove the capped organic residues. The difference between the final total weight and the weight of the vial is correlative to the mass of c-In_2O_3 nanoctahedra in 1.0 mL of stock suspension. (2) The as-prepared Pd nanoparticles were further washed twice using a pair of anhydrous ethanol−hexane (polar−nonpolar) solvents followed by centrifugation, and finally redispersed in toluene containing 1-dodecanethiol (≥98%, Singma-Aldrich). The volume ratio between 1-dodecanethiol and toluene was 0.0125:1. The concentration of this toluene stock suspension was estimated using the same procedure as mentioned above.

Preparation of BNSLs on TEM Grids. A 50 μL portion of c-In_2O_3 nanoctahedron stock suspension in toluene (7.2×10^{-3} M) was completely mixed with 20 μL of Pd stock suspension in toluene (3.8×10^{-3} M) and 3 μL of oleic acid in a vial. Assembly of such a mixture was conducted on copper TEM grids coated with Formvar/carbon under ambient conditions (200 Mesh, Ted Pella Inc.).

Acknowledgment. This work was partially supported by NSF CAREER program (DMR-0731382), S^3IP and State University of New York at Binghamton. The structural modeling was done using MS modeling 5.0 through Laboratory for Molecular Simulation, Department of Chemistry, Texas A&M University.

Supporting Information Available: TEM images of 2 structured c-In_2O_3-Pd 2D BNSLs, TEM images at various tilting angles, and reconstructed tomographic image at the same area; movies of BNSL aligned TEM image during the tilting experiment and 3D reconstructed isosurface volume, visualizing the positions of Pd NPs to c-In_2O_3 nanoctahedra in the BNSLs in a round turn. These materials are available free of charge *via* the Internet at http://pubs.acs.org.

REFERENCES AND NOTES

1. Lee, H.; Habas, S. E.; Kweskin, S.; Butcher, D.; Somorjai, G. A.; Yang, P. Morphological Control of Catalytically Active Platinum Nanocrystals. *Angew. Chem. Int. Ed.* **2006**, *45*, 7824–7828.
2. Xiong, Y.; Cai, H.; Wiley, B. J.; Wang, J.; Kim, M. J.; Xia, Y. Synthesis and Mechanistic Study of Palladium Nanobars and Nanorods. *J. Am. Chem. Soc.* **2007**, *129*, 3665–3675.
3. Wang, C.; Daimon, H.; Onodera, T.; Koda, T.; Sun, S. A General Approach to the Size- and Shape-Controlled Synthesis of Platinum Nanoparticles and Their Catalytic Reduction of Oxygen. *Angew. Chem. Int. Ed.* **2008**, *47*, 3588–3591.
4. Dumestre, F.; Chaudret, B.; Amiens, C.; Renaud, P.; Fejes, P. Superlattices of Iron Nanocubes Synthesized from $Fe[N(SiMe_3)_2]_2$. *Science* **2004**, *303*, 821–823.
5. Milliron, D. J.; Hughes, S. M.; Cui, Y.; Manna, L.; Li, J.; Wang, L.-W.; Alivisatos, A. P. Colloidal Nanocrystal Heterostructures with Linear and Branched Topology. *Nature* **2004**, *430*, 190–195.
6. Chen, O.; Chen, X.; Yang, Y.; Lynch, J.; Wu, H.; Zhuang, J.; Cao, Y. C. Synthesis of Metal−Selenide Nanocrystals Using Selenium Dioxide as the Selenium Precursor. *Angew. Chem. Int. Ed.* **2008**, *47*, 8638–8641.
7. Joo, J.; Na, H. B.; Yu, T.; Yu, J. H.; Kim, Y. W.; Wu, F.; Zhang, J. Z.; Hyeon, T. Generalized and Facile Synthesis of Semiconducting Metal Sulfide Nanocrystals. *J. Am. Chem. Soc.* **2003**, *125*, 11100–11105.
8. Kagan, C. R.; Murray, C. B.; Bawendi, M. G. Long-Range Resonance Transfer of Electronic Excitations in Close-packed CdSe Quantum-Dot Solids. *Phys. Rev. B* **1996**, *54*, 8633–8643.
9. Shevchenko, E. V.; Talapin, D. V.; O'Brien, S.; Murray, C. B. Polymorphism in AB_{13} Nanoparticle Superlattices: An Example of Semiconductor-Metal Metamaterials. *J. Am. Chem. Soc.* **2005**, *127*, 8741–8747.
10. Redl, F. X.; Cho, K.-S.; Murray, C. B.; O'Brien, S. Three-Dimensional Binary Superlattices of Magnetic Nanocrystals and Semiconductor Quantum Dots. *Nature* **2003**, *423*, 968–971.
11. Rogach, A. L.; Talapin, D. V.; Shevchenko, E. V.; Kornowski, A.; Haase, M.; Weller, H. Organization of Matter on Different Size Scales: Monodisperse Nanocrystals and Their Superstructures. *Adv. Funct. Mater.* **2002**, *12*, 653–664.
12. Kiely, C. J.; Fink, J.; Brust, M.; Bethell, D.; Schiffrin, D. J. Spontaneous Ordering of Bimodal Ensembles of Nanoscopic Gold Clusters. *Nature* **1998**, *396*, 444–446.
13. Collier, C. P.; Vossmeyer, T.; Heath, J. R. Nanocrystal Superlattices. *Annu. Rev. Phys. Chem.* **1998**, *49*, 371–404.
14. Zhuang, Z.; Peng, Q.; Zhang, B.; Li, Y. Controllable Synthesis of Cu_2S Nanocrystals and Their Assembly into a Superlattice. *J. Am. Chem. Soc.* **2008**, *130*, 10482–10483.
15. Shevchenko, E. V.; Talapin, D. V.; Kotov, N. A.; O'Brien, S.; Murray, C. B. Structural Diversity in Binary Nanoparticle Superlattices. *Nature* **2006**, *439*, 55–59.
16. Shevchenko, E. V.; Talapin, D. V.; Murray, C. B.; O'Brien, S. Structural Characterization of Self-Assembled Multifunctional Binary Nanoparticle Superlattices. *J. Am. Chem. Soc.* **2006**, *128*, 3620–3637.
17. Chen, Z.; O'Brien, S. Structure Direction of II−VI Semiconductor Quantum Dot Binary Nanoparticle Superlattices by Tuning Radius Ratio. *ACS Nano* **2008**, *2*, 1219–1229.
18. Eldridge, M. D.; Madden, P. A.; Frenkel, D. Entropy-Driven Formation of a Superlattice in a Hard-Sphere Binary Mixture. *Nature* **1993**, *365*, 35–37.
19. Bartlett, P.; Ottewill, R. H.; Pusey, P. N. Superlattice Formation in Binary Mixtures of Hard-Sphere Colloids. *Phys. Rev. Lett.* **1992**, *68*, 3801–3804.
20. Evers, W. H.; Friedrich, H.; Filion, L.; Dijkstra, M.; Vanmaekelbergh, D. Observation of a Ternary Nanocrystal Superlattice and Its Structural Characterization by Electron Tomography. *Angew. Chem. Int. Ed.* **2009**, *48*, 9655–9657.
21. Xu, D.; Bliznakov, S.; Liu, Z.; Fang, J.; Dimitrov, N. Composition-Dependent Electrocatalytic Activity of Pt−Cu Nanocube Catalysts towards Formic Acid Oxidation. *Angew. Chem. Int. Ed.* **2010**, *49*, 1282–1285.
22. Christopher, P.; Linic, S. Shape- and Size-Specific Chemistry of Ag Nanostructures in Catalytic Ethylene Epoxidation. *ChemCatChem.* **2010**, *2*, 78–83.
23. Bratlie, K. M.; Lee, H.; Komvopoulos, K.; Yang, P.; Somorjai, G. A. Platinum Nanoparticle Shape Effects on Benzene Hydrogenation Selectivity. *Nano Lett.* **2007**, *7*, 3097–3101.
24. Narayanan, R.; El-Sayed, M. A. Some Aspects of Colloidal Nanoparticle Stability, Catalytic Activity, and Recycling Potential. *Top. Catal.* **2008**, *47*, 15–21.
25. Zeng, H.; Li, J.; Liu, J. P.; Wang, Z. L.; Sun, S. Exchange-Coupled Nanocomposite Magnets by Nanoparticle Self-Assembly. *Nature* **2002**, *420*, 395–398.
26. Mcguire, J. A.; Joo, J.; Pietryga, J. M.; Schaller, R. D.; Klimov, V. I. New Aspects of Carrier Multiplication in Semiconductor Nanocrystals. *Acc. Chem. Res.* **2008**, *41*, 1810–1819.
27. Nozik, A. J. Multiple Exciton Generation in Semiconductor Quantum Dots. *Chem. Phys. Lett.* **2008**, *457*, 3–11.
28. Luther, J. M.; Law, M.; Beard, M. C.; Song, Q.; Reese, M. O.; Ellingson, R. J.; Nozik, A. J. Schottky Solar Cells Based on Colloidal Nanocrystal Films. *Nano Lett.* **2008**, *8*, 3488–3492.
29. Luther, J. M.; Law, M.; Song, Q.; Perkins, C. L.; Beard, M. C.;

Nozik, A. J. Structural, Optical, and Electrical Properties of Self-Assembled Films of PbSe Nanocrystals Treated with 1,2-Ethanedithiol. *ACS Nano* **2008**, *2*, 271–280.
30. Lu, W.; Liu, Q.; Sun, Z.; He, J.; Ezeolu, C.; Fang, J. Super Crystal Structures of Octahedral c-In_2O_3 Nanocrystals. *J. Am. Chem. Soc.* **2008**, *130*, 6983–6991.
31. Kim, S.-W.; Park, J.; Jang, Y.; Chung, Y.; Hwang, S.; Hyeon, T. Synthesis of Monodisperse Palladium Nanoparticles. *Nano Lett.* **2003**, *3*, 1289–1291.
32. Shim, M.; Guyot-Sionnest, P. Permanent Dipole Moment and Charges in Colloidal Semiconductor Quantum Dots. *J. Chem. Phys.* **1999**, *111*, 6855–6964.
33. Krauss, T. D.; Brus, L. E. Charge, Polarizability, and Photoionization of Single Semiconductor Nanocrystals. *Phys. Rev. Lett.* **1999**, *83*, 4840–4843.
34. Islam, M. A.; Herman, I. P. Electrodeposition of Patterned CdSe Nanocrystal Films Using Thermally Charged Nanocrystals. *Appl. Phys. Lett.* **2002**, *80*, 3823–3825.
35. O'Brien, R. W.; White, L. R. Electrophoretic Mobility of a Spherical Colloidal Particle. *J. Chem. Soc., Faraday Trans. 2* **1978**, *74*, 1607–1626.
36. Williams, D. B.; Carter, C. B. *Transmission Electron Microscopy*; Spectrometry, Vol. 4; Plenum Press: New York, 1996.
37. Beiser, A. *Physics*; 4th ed.; Addison-Wesley Publishing Company: Reading, MA, 1986.